Solution Studies of Staphylococcal Nuclease H124L. 2. ^{1}H, ^{13}C, and ^{15}N Chemical Shift Assignments for the Unligated Enzyme and Analysis of Chemical Shift Changes That Accompany Formation of the Nuclease–Thymidine 3′,5′-Bisphosphate–Calcium Ternary Complex[†,‡]

Jinfeng Wang,[§] Andrew P. Hinck,[§] Stewart N. Loh,[§] David M. LeMaster,[∥] and John L. Markley*[,§]

Department of Biochemistry and National Magnetic Resonance Facility at Madison, College of Agricultural and Life Sciences, University of Wisconsin, 420 Henry Mall, Madison, Wisconsin 53706, and Department of Biochemistry, Molecular Biology and Cell Biology, Northwestern University, Evanston, Illinois 60208

Received June 4, 1991; Revised Manuscript Received September 20, 1991

ABSTRACT: Accurate ^{1}H, ^{15}N, and ^{13}C chemical shift assignments were determined for staphylococcal nuclease H124L (in the absence of inhibitor or activator ion). Backbone ^{1}H and ^{15}N assignments, obtained by analysis of three-dimensional ^{1}H–^{15}N HMQC-NOESY data [Wang, J., Mooberry, E. S., Walkenhorst, W. F., & Markley, J. L. (1992) *Biochemistry* (preceding paper in this issue)], were refined and extended by a combination of homo- and heteronuclear two-dimensional NMR experiments. Staphylococcal nuclease H124L samples used in the homonuclear ^{1}H NMR studies were at natural isotopic abundance or labeled randomly with ^{2}H (to an isotope level of 50%); nuclease H124L samples used for heteronuclear NMR experiments were labeled uniformly with ^{15}N (to an isotope level >95%) or uniformly with ^{13}C (to an isotope level of 26%). Additional nuclease H124L samples were labeled selectively by incorporating single ^{15}N- or ^{13}C-labeled amino acids. The chemical shifts of uncomplexed enzyme were then compared with those determined previously for the nuclease H124L·pdTp·Ca^{2+} ternary complex [Wang, J., LeMaster, D. M., & Markley, J. L. (1990) *Biochemistry 29*, 88–101; Wang, J., Hinck, A. P., Loh, S. N., & Markley, J. L. (1990) *Biochemistry 29*, 102–113; Wang, J., Hinck, A. P., Loh, S. N., & Markley, J. L. (1990) *Biochemistry 29*, 4242–4253]. The results reveal that the binding of pdTp and Ca^{2+} induces large shifts in the resonances of several amino acid segments. These chemical shift changes are interpreted in terms of changes in backbone torsion angles that accompany the binding of pdTp and Ca^{2+}; changes at the binding site appear to be transmitted to other regions of the molecule through networks of hydrogen bonds.

Staphylococcal nuclease (EC 3.1.31.1) has been widely studied as a model for protein folding and for enzymatic structure–function relationships. The enzyme requires Ca^{2+} for activity and is inhibited competitively by the mononucleotide bisphosphate, pdTp[1] in the presence of Ca^{2+} (Cunningham et al., 1956). The nuclease·pdTp·Ca^{2+} ternary complex has been studied by X-ray crystallography (Loll & Lattman, 1989; Tucker et al., 1979a) and by NMR spectroscopy (Wang et al., 1990a–c; Torchia et al., 1989). Staphylococcal nuclease undergoes a local conformational change when pdTp and Ca^{2+} are bound (Markley & Jardetzky, 1970). The positions of certain residues in the neighborhood of the pdTp- and Ca^{2+}-binding sites change upon ternary complex formation (Tucker et al., 1979b). Formation of the ternary complex also shifts the equilibrium between the a1 (cis Lys^{116}–Pro^{117} peptide bond) and a2 (trans Lys^{116}–Pro^{117} peptide bond) conformational substates that are present in solution;

[†] Supported by NIH Grant GM 35976. NMR studies were carried out in the National Magnetic Resonance Facility at Madison, which is supported by NIH Grant RR02301. Equipment in the NMR Facility was purchased with funds from the NIH Biomedical Research Technology Program (Grant RR02301), the University of Wisconsin, the National Science Foundation Biological Instrumentation Program (Grant DMB-8415048), the NIH Shared Instrumentation Program (Grant RR02781), and the U.S. Department of Agriculture. A.P.H. is a trainee on NIH Molecular Biophysics Training Grant 5 T32 GM08293; S.N.L is a trainee on NIH Cell and Molecular Biology Training Grant 5 T32 GM07215.

[‡] NMR data were deposited in BioMagResBank (Ulrich et al., 1989) under ref ID 957.

[§] University of Wisconsin—Madison.

[∥] Northwestern University.

[1] Abbreviations: a1, subconformation of nuclease whose relative abundance increases upon pdTp and Ca^{2+} binding [this subconformation has a cis Lys^{116}–Pro^{117} peptide bond (Alexandrescu et al., 1989; Wang et al., 1990c)]; a2, subconformation of nuclease whose relative abundance decreases upon pdTp and Ca^{2+} binding [this subconformation has a trans Lys^{116}–Pro^{117} peptide bond (Alexandrescu et al., 1989; Wang et al., 1990c)]; DQF-COSY, 2D double-quantum filtered correlated spectroscopy; [na]H124L, natural abundance nuclease H124L; [50% UL ^{2}H]-H124L, 50% random fractionally deuterated nuclease H124L; [26% UL ^{13}C]H124L, nuclease H124L enriched uniformly with ^{13}C to 26% isotope; [26% UL ^{13}C]His-H124L, nuclease H124L whose histidine residues have been enriched uniformly with ^{13}C to 26% isotope; [95% UL ^{15}N]H124L, nuclease H124L enriched uniformly with ^{15}N to >95% isotope; [95% UL ^{15}N]His-H124L, nuclease H124L containing histidine enriched uniformly with ^{15}N to >95% isotope; HOHAHA, 2D ^{1}H homonuclear Hartmann–Hahn magnetization transfer spectroscopy; MBC, 2D multiple-bond correlation; NMR, nuclear magnetic resonance; NOE, nuclear Overhauser enhancement; NOESY, 2D NOE spectroscopy; NOESY-HMQC, nuclease Overhauser–multiple-quantum coherence spectroscopy; nuclease H124L, recombinant protein produced in *Escherichia coli* whose sequence is identical to that of the nuclease from the V8 strain of *Staphylococcus aureus*; pdTp, thymidine 3′,5′-bisphosphate; pH*, direct pH meter reading taken of a sample dissolved in $^{2}H_2O$; TMS, tetramethylsilane; TSP, 3-(trimethylsilyl)propionate-d_4; RCT-COSY, 2D relayed coherence transfer spectroscopy; RMS, root mean square; UL, uniformly labeled; SBC, single-bond correlation; SBC-NOE, 2D single-bond correlation with NOE relay; 2D, two dimensional; 3D, three dimensional. Cross peak positions in 2D spectra are given as (x,y) ppm, where x is the horizontal axis and y is the vertical axis.

0006-2960/92/0431-921$03.00/0

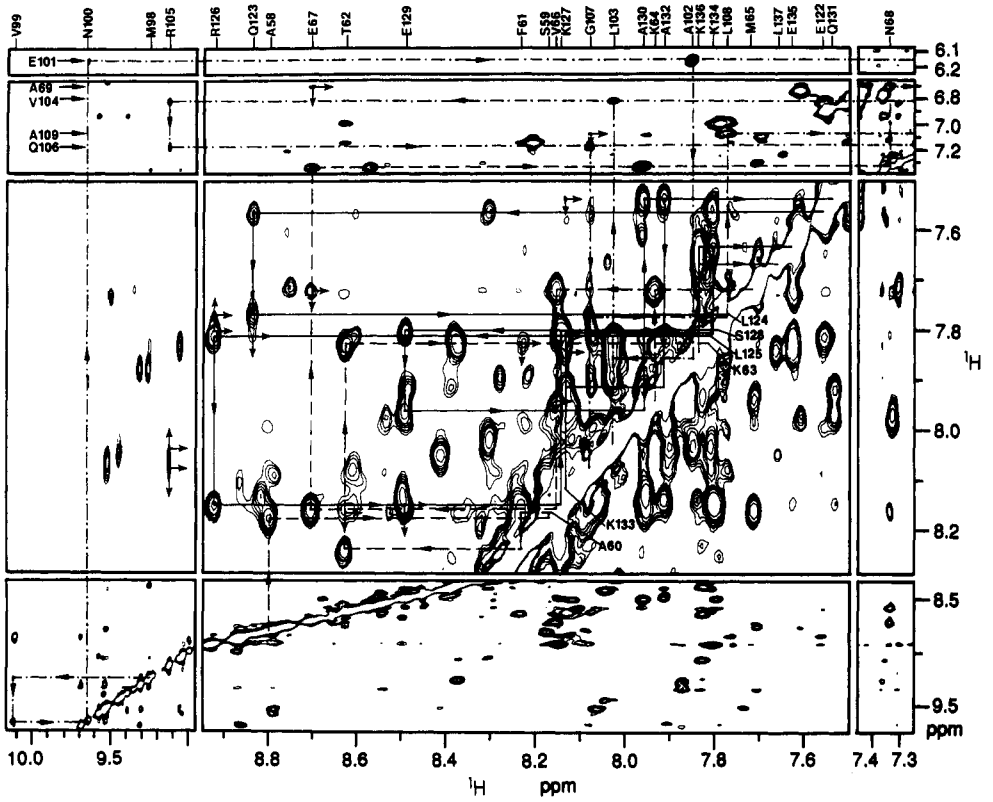

FIGURE 1: Portions of the 600-MHz NOESY spectrum of [50% UL ^{2}H]H124L in H_2O solution. The spectrum was recorded with 700 values in t_1 and with 140 acquisitions per t_1 value. The NOE mixing time was 250 ms. A total of 4096 points were collected in the t_2 dimension, and the t_1 dimension was extended from 700 to 4096 points by zero-filling. A Gaussian weighting function was used in the t_2 dimension, and a shifted sine bell window function was applied in the t_1 dimension. Three long chains of sequential d_{NN} connectivities provide evidence for three separate α-helices as indicated by dashed lines (A58–A69), dotted-dashed lines (M98–A109), and solid lines (E122–L137). Long-range $d_{NN}(i,i+2)$ NOE's are indicated by arrows at right angles.

both forms bind inhibitor, but since the a1 form binds inhibitor more tightly than the a2 form, the equilibrium shifts toward a1 (Alexandrescu et al., 1989; Wang et al., 1990c).

One approach to determining the location of protein conformational changes that occur upon ligand binding is to map out those nuclei that undergo NMR chemical shift changes on complex formation. Although chemical shift changes are usually difficult to interpret in structural terms, they are a sensitive indicator of the positions at which structural changes occur.

The chemical shifts of (unligated) nuclease H124L are compared here with those of the H124L·pdTp·Ca^{2+} ternary complex. The ^{1}H, ^{15}N, and ^{13}C chemical shifts of the nuclease H124L ternary complex were determined previously by multinuclear 2D NMR spectroscopy (Wang et al., 1990a–c). We initially tried to use the same 2D NMR assignment strategy with unligated nuclease H124L. However, cross peaks in the 2D ^{1}H COSY (H_2O) and NOESY (H_2O) NMR spectra of uncomplexed nuclease H124L are broader and more overlapped than those of the ternary complex, and this created difficulties in assigning several parts of the 2D spectra. For this reason, we found it expedient to determine the sequential connectivities from 3D ^{1}H–^{15}N NOESY-HMQC data (Wang et al., 1992). Sequential $^1H^N_i$–$^1H^N_{i+1}$ (d_{NN}) connectivities in the 2D ^{1}H{^{1}H}NOESY and ^{1}H{^{15}N}SBC-NOE spectra (H_2O) could then be followed by reference to these assignments so that the ^{1}H and ^{15}N chemical shifts of residues involved in three long α-helical segments could be refined. By following $^1H^\alpha_i$–$^1H^N_{i+1}$ ($d_{\alpha N}$) connectivities, it was possible to extend the assignments of the three antiparallel β-sheets and other segments. The strategy used to determine atom-specific ^{15}N and ^{13}C assignments from 2D ^{1}H{^{13}C,^{15}N} heteronuclear correlated NMR spectra was that used previously with the ternary complex (Wang et al., 1990b,c). The added chemical shift dimension in the 3D ^{1}H–^{15}N NOESY-HMQC spectrum gives good peak separations, but the accuracy of chemical shift determinations in all dimensions is lower than in 2D spectra. Several 3D peaks whose ^{1}H or ^{15}N chemical shifts appeared equivalent were found to have measurably different chemical shifts by analysis of 2D spectra.

This paper describes (1) the homonuclear ^{1}H NMR experiments used to identify the spin systems of individual residues for use in positioning the main-chain connectivity patterns of the 3D ^{1}H–^{15}N NOESY-HMQC data [described in the accompanying paper, Wang et al. (1992)], (2) the ^{1}H NOESY, ^{1}H{^{13}C}SBC, ^{1}H{^{13}C}SBC-NOE, ^{1}H{^{15}N}SBC, and ^{1}H{^{15}N}SBC-NOE spectral data used to correlate the sequential and full intraresidue assignments, (3) the refinement of the chemical shifts of the main-chain ^{1}H and ^{15}N nuclei (whose sequential assignments were determined from the 3D data) by tracing out the assignment pathways in 2D spectra, and (4) quantitative analysis of the chemical shift changes that accompany ternary complex formation.

Experimental Procedures

Protein Samples. Two nuclease samples having different isotopic compositions were used in the homonuclear ^{1}H 2D NMR studies: 3.5 mM [na]H124L in 100% ^2H_2O and 4.5 mM [50% UL ^{2}H]H124L in 90% H_2O/10% ^2H_2O. Four nuclease samples having different isotopic compositions were used in the heteronuclear 2D NMR studies: 5 mM [26% UL ^{13}C]H124L in 100% ^2H_2O, 5 mM [26% UL ^{13}C]His-H124L in 100% ^2H_2O, 5 mM [95% UL ^{15}N]H124L in 90% H_2O/10%

^2H_2O, and 5 mM [95% UL ^{15}N]His-H124L in 100% ^2H_2O. The preparation and purification the nuclease samples of different isotopic composition were described previously: [na]H124L and [50% UL ^2H]H124L (Wang et al., 1990a); ^{13}C- and ^{15}N-labeled samples (Wang et al., 1990b). All solutions contained 0.3 M KCl. The pH of samples dissolved in H_2O was 5.1, and the pH* of samples dissolved in ^2H_2O was 5.5.

NMR Spectroscopy. Homonuclear and heteronuclear 2D ^1H–^1H, ^1H–^{13}C, and ^1H–^{15}N NMR spectra were recorded on Bruker AM-500 (11.8 tesla) or AM-600 (14.1 tesla) spectrometers at a temperature setting of 45 °C. ^1H chemical shifts were measured relative to the major signal of internal TSP (defined as 0 ppm). 2D ^1H NMR spectra of protein samples in 100% ^2H_2O were calibrated by assigning the first diagonal peak in the aromatic region (assigned to $^1H^\epsilon$ of Y91) a chemical shift value of 6.58 ppm relative to internal TSP; the chemical shift of this peak was determined from the 1D ^1H spectrum. 2D ^1H NMR spectra of samples dissolved in 90% H_2O/10% ^2H_2O were calibrated by assigning the clearly resolved diagonal peak from amino acid residue E101 a chemical shift value of 6.17 ppm; this chemical shift had been determined from a 1D ^1H spectrum. ^{13}C chemical shifts were measured from 10% external dioxane in ^2H_2O, which was assumed to be at 67.8 ppm relative to the chemical shift reference, TMS. ^{15}N chemical shifts were measured from 95% $(^{15}NH_4)_2SO_4$ in 90% H_2O/10% ^2H_2O, which was assumed to be at 21.6 ppm relative to the chemical shift reference, liquid ammonia.

Two-dimensional $^1H\{^1H\}$ phase-sensitive DQF-COSY (Rance et al., 1983) and HOHAHA (Bax & Davis, 1985) spectra were acquired with [na]H124L. $^1H\{^1H\}$ phase-sensitive COSY and RCT-COSY (Wagner, 1983; Bax & Drobny, 1985) spectra were recorded with [50% UL ^2H]H124L. ^1H-$\{^1H\}$ phase-sensitive NOESY data (Anil Kumar et al., 1980; Bodenhausen et al., 1984) were obtained from both [na]H124L and [50% UL ^2H]H124L samples. Nuclease samples labeled uniformly with ^{13}C or ^{15}N were used for the heteronuclear SBC (Sklenar et al., 1987) and SBC-NOE (Shon & Opella, 1989) experiments. On the other hand, nuclease samples labeled selectively with ^{13}C or ^{15}N at certain positions were used in the 2D heteronuclear MBC experiments (Bax et al., 1986). The pulse sequences used in this study were as described in the studies of the nuclease H124L ternary complex (Wang et al., 1990a–c). Additional experimental details are given in the figure legends.

Results

Preliminary comparisons of the NMR data from uncomplexed nuclease H124L [^1H NOESY (Figure 1), ^1H HOHAHA (^2H_2O), RCT-COSY (H_2O) (not shown), DQF-COSY (^2H_2O) (Figure 2), and COSY (H_2O, fingerprint region) (Figure 3)] led to spin system analyses of all Thr, Ala, and Val residues and some Gly, Ser, Ile, and aromatic residues.

α-Helical Domains: Ala^{58} to Ala^{69}, Met^{98} to Ala^{109}, and Glu^{122} to Leu^{137}

(1) Sequence-Specific Assignment of Backbone ^1H Signals. Three long continuous stretches of strong sequential d_{NN} NOE connectivities found in the ^1H–^1H NOESY (H_2O) spectrum of [50% UL ^2H]H124L are shown in Figure 1. The ^1H $d_{NN}(i,i+2)$ NOE's are designated by arrows that point to the positions of the corresponding residues. Dashed lines represent the sequential d_{NN} walk from A58 to A69. Dotted-dashed lines illustrate sequential d_{NN} NOE connectivities from M98 to

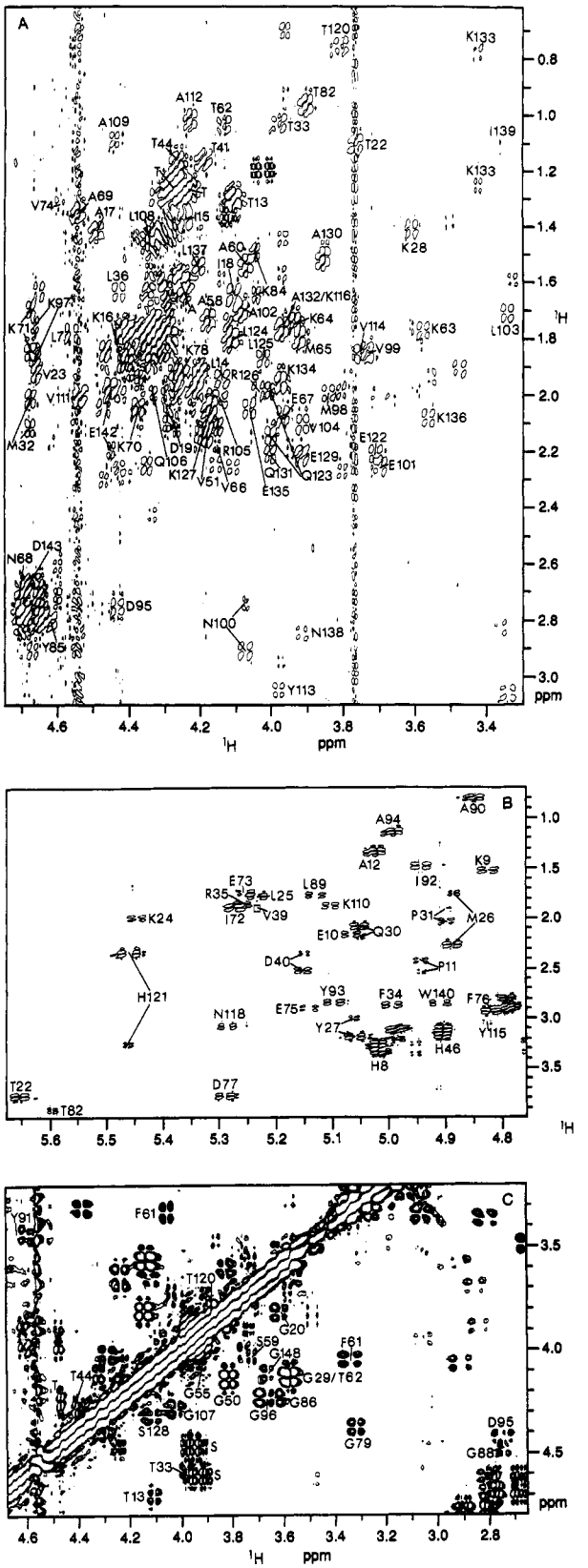

FIGURE 2: Selected aliphatic regions of 500-MHz phase-sensitive DQF-COSY spectra of nuclease samples. The spectra were recorded with a 6500-Hz spectral width, and 4096 points were collected in t_2. The t_1 domain was extended to 4096 points by zero-filling. Sine bell window functions were used in both dimensions. Identified cross peaks are labeled with the sequence number and one-letter amino acid code. (A and B) [50% UL ^2H]H124L in ^2H_2O solution. A total of 700 t_1 increments were collected; 168 scans were accumulated at each t_1 value. (C) [na]H124L in ^2H_2O solution. The spectrum was recorded with 512 values in t_1 and 128 scans for each t_1 value.

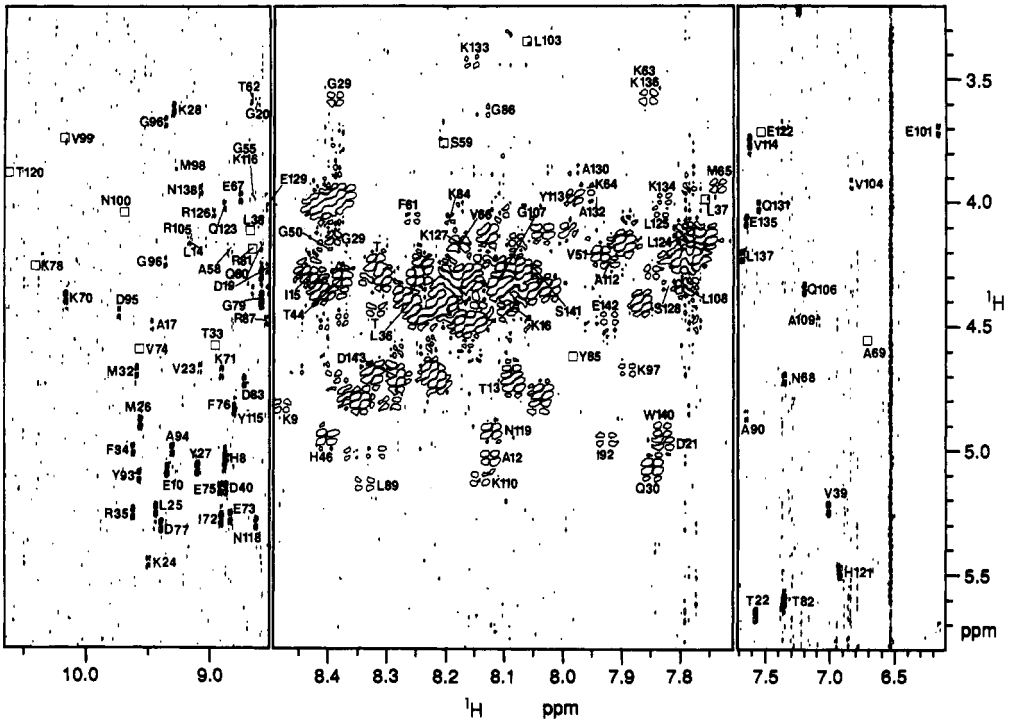

FIGURE 3: Fingerprint region of the 600-MHz phase-sensitive COSY spectrum of [50% UL ^{2}H]H124L in ^2H_2O solution. The spectrum was recorded with 700 increments in t_1, and 4096 points were collected in t_2. A total of 140 scans were accumulated for each t_1 value. Sine bell window functions were applied in both dimensions. The t_1 dimension was extended to 4096 points by zero-filling prior to Fourier transformation. Assigned cross peaks are indicated by the one-letter amino acid code with residue number. Boxes indicate the positions of cross peaks that are visible at lower contour levels than those plotted here (or are missing in this spectrum).

A109. Solid lines show the longest stretch of sequential d_{NN} connectivities, from E122 to L137. [The sequential $d_{\alpha N}$ and $d_{\alpha N}(i,i+3)$ NOE connectivities identified within these three segments are shown in Figure 1S of the Supplementary Material.]

The sequential d_{NN} NOE connectivities between S59 and A60 and between L124 and L125 were not observed in the 2D ^{1}H NOESY spectrum (Figure 1) since they are buried in the diagonal. The sequential assignments were derived from the 3D data because these residues have different amide ^{15}N chemical shifts. Assigned cross peaks in the fingerprint region of the ^{1}H COSY (H_2O) spectrum are indicated in Figure 3.

(2) Sequence-Secific Assignment of Backbone ^{15}N Signals. Figure 4 shows the ^{1}H–^{15}N connectivity region of the 2D ^{1}H{^{15}N}SBC spectrum of [95% UL ^{15}N]H124L. Assigned ^{1}H–^{15}N direct connectivity peaks are labeled in this figure. The corresponding region of the 2D ^{1}H{^{15}N}SBC-NOE spectrum of the same sample shows additional NOE relay cross peaks that provide ^{15}N-assisted sequential d_{NN} connectivities (Wang et al., 1990b) for the three long α-helices (Figure 2S, Supplementary Material). The ^{1}H chemical shifts from these ^{1}H–^{15}N cross peaks match those assigned in the ^{1}H NOESY data (Figure 1); ^{15}N chemical shifts from these cross peaks match those assigned to the $^1H^{\beta}$–^{15}N region of the same ^{1}H-{^{15}N}SBC-NOE spectrum (Figure 5).

(3) Site-Specific Assignment of β-Proton Signals. The $^1H^{\beta}$–^{15}N region of the ^{1}H{^{15}N}SBC-NOE spectrum of [95% UL ^{15}N]H124L provides the same information as that obtained from the $^1H^{\beta}$–$^1H^N$ connectivity region of the ^{1}H RCT-COSY (H_2O), and NOESY (H_2O) spectra. Since strong $d_{\beta N}(i,i)$ and sequential $d_{\beta N}(i,i+1)$ NOE connectivities are characteristics of α-helix (Englander et al., 1987), three long sequential $d_{\beta N}$ walks are expected. Figure 5 shows three stretches of strong, sequential $d_{\beta N}$ NOE's: E122–L137 (dashed lines), A58–A69 (dotted-dashed lines), and V99–Q106 (solid lines). The chemical shift assignments of the β-protons of these

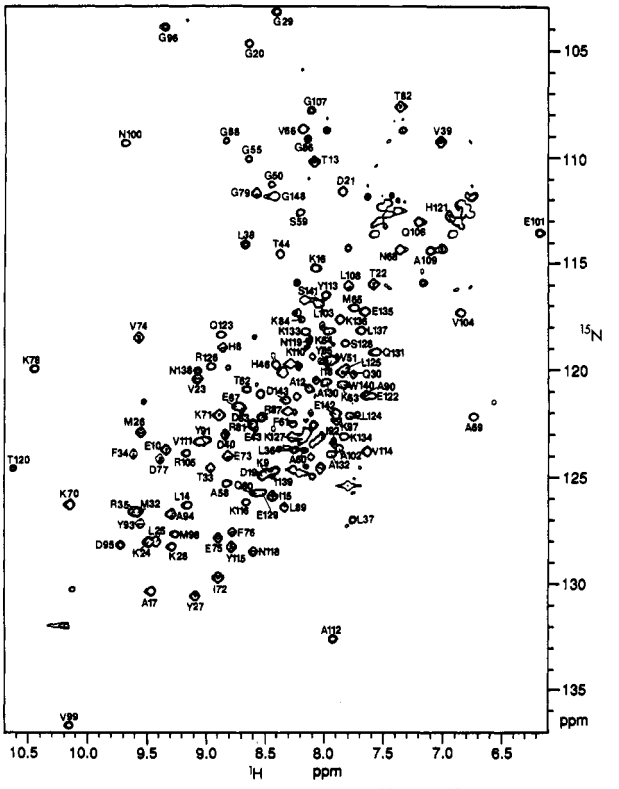

FIGURE 4: Assignments of backbone $^1H^N$ and ^{15}N signals in the $^1H^N$–^{15}N connectivity regions of the 600-MHz ^{1}H{^{15}N}SBC spectrum of [95% UL ^{15}N]H124L in H_2O solution. Data were collected with 4096 points in t_2. A total of 344 t_1 increments were collected with 176 scans for each. Zero-filling was applied in t_1 to extend it to 2048 points. A Gaussian function was used in t_2, and a shifted sine bell function was used in t_1. The assigned cross peaks are labeled.

three helices are consistent with the approximate values determined from the 3D ^{1}H–^{15}N NOESY-HMQC data (Wang

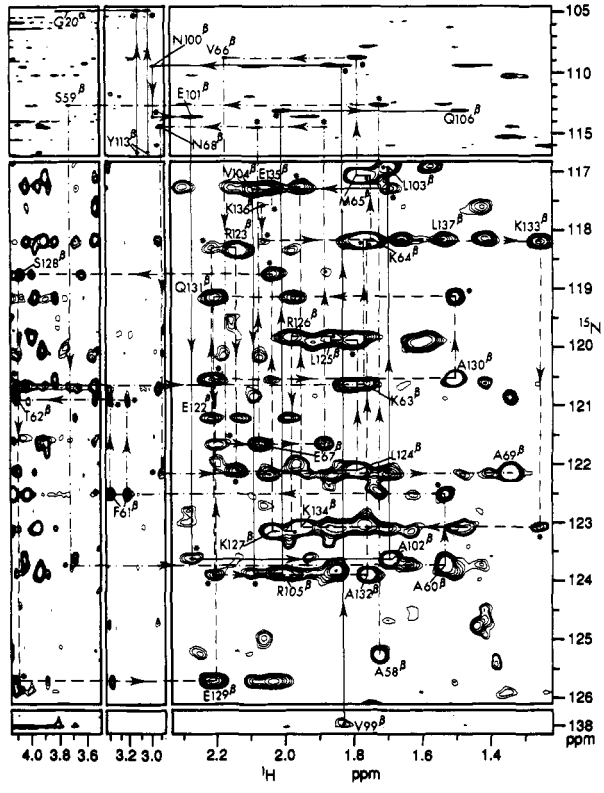

FIGURE 5: $^1H^{\beta}$–^{15}N connectivity regions of the 600-MHz $^1H\{^{15}N\}$-SBC-NOE spectrum of [95% UL ^{15}N]H124L in H_2O solution. A total of 396 t_1 increments were collected with 208 scans for each. The NOE mixing time was set to 250 ms. Other parameters were as indicated in the legend to Figure 4. Three ^{15}N-assisted sequential $d_{\beta N}$ NOE connectivities were assigned to V99–Q106 (solid lines), A58–A69 (dotted-dashed lines), and E122–L137 (dashed lines). The interresidue NOE relay cross peaks are indicated by asterisks. The assigned $^1H^{\beta}$–^{15}N NOE relay cross peaks are labeled.

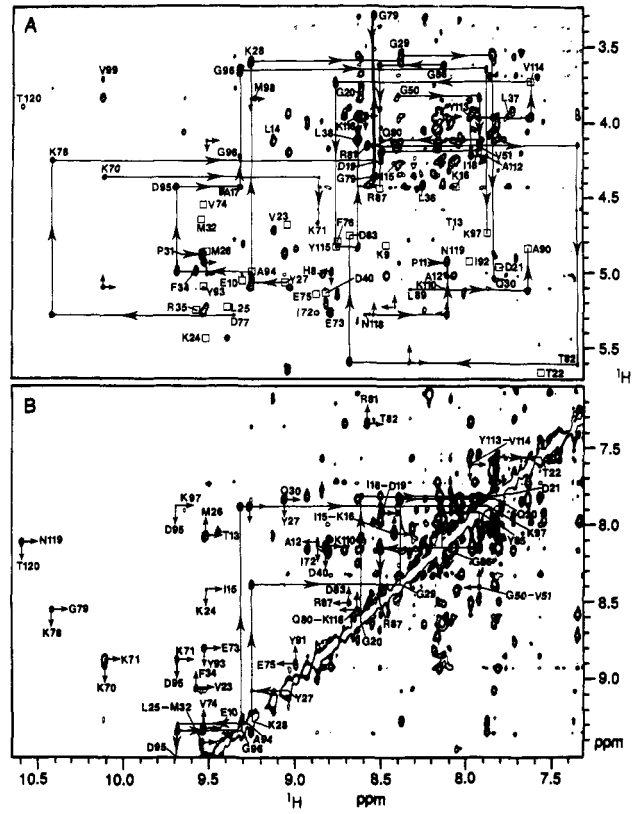

FIGURE 6: Portions of the 600-MHz ^1H NOESY spectrum of [50% UL ^2H]H124L in H_2O solution. (A) The $d_{\alpha N}$ connectivity region. Solid lines indicate the $d_{\alpha N}$ NOE connectivities of turns and loops. The positions of corresponding COSY cross peaks are indicated by boxes. Arrows at right angles indicate $d_{\alpha N}(i,j+1)$ or $d_{\alpha N}(j,i+1)$ NOE cross peaks between opposite strands. (B) The d_{NN} NOE connectivities that provide evidence for turns and loops. The positions of corresponding COSY cross peaks are indicated by small boxes. Long-range NOE's between two opposite strands or between residues of the turns are indicated by arrows at right angles.

et al., 1992). Assigned $^1H^{\alpha}$–$^1H^{\beta}$ cross peaks in the ^1H DQF-COSY (^2H_2O) spectrum from residues in the three α-helical segments are indicated in Figure 2.

Antiparallel β-Sheets: His[8] to Arg[35], Leu[38] to Thr[41], Ile[72] to Phe[76], Ala[90] to Val[99], and Ala[109] to Ala[112]

A schematic representation of the β-structure, which incorporates NOE's detected in both the 2D and 3D data, is shown in the previous paper (Wang et al., 1992; Figure 6).

(1) Sequence-Specific Assignment of Backbone ^1H Signals. Resonances from backbone protons within antiparallel β-sheet were assigned on the basis of characteristic NOE cross peaks (Englander et al., 1987): long stretches of strong, sequential $d_{\alpha N}$ connectivities in the ^1H NOESY (^1H_2O) spectrum. The reverse turns (Richardson, 1981) that form part of the antiparallel β-structure were determined from patterns of ^1H–^1H NOE's (Wagner et al., 1986).

According to information from the 3D ^1H–^{15}N NOESY-HMQC NMR spectrum (Wang et al., 1992), segments H8–A12, I72–F76, and A90–V99 constitute an antiparallel β-sheet structure with a reverse turn at A94–D95–G96–K97. The A12–R35 segment was found to form an antiparallel β-sheet structure with turns at Y27–K28–G29–Q30 and I18–D19–G20–D21. Segments L38–T41 and A109–A112 constitute a small piece of antiparallel β-sheet. The intra- and interresidue NOE cross peaks of these three β-sheets can be seen in Figure 6A. Although cross peaks from T41, Y91, and V111 are missing in the COSY fingerprint region (Figure 3), backbone assignments to these residues are provided by the $^1H\{^{15}N\}$SBC and $^1H\{^{15}N\}$SBC-NOE data (discussed below). Linkage of the intra- and interresidue NOE cross peaks within these three β-sheets (Figure 6A) predicted the observed sequential $d_{\alpha N}$ connectivities (Figure 3S, Supplementary Material).

Of the five isoleucine spin systems of nuclease H124L, three (I15, I72, and I92) were identified from $d_{\alpha N}$ sequential walks (Figure 3S) and by reference to the ^1H–^{15}N 3D data (Wang et al., 1992). The fourth, which showed shielded chemical shifts, was assigned tentatively to I139 in analogy with results from the ternary complex which showed that this residue is shielded by an interaction with the aromatic ring of W140 (Wang et al., 1990c). Placement of the signals from the remaining isoleucine spin system (I18) led to identification of $d_{\alpha N}$ and d_{NN} NOE connectivities linking I18 to D19 (Figure 6A,B). Since residue 31 is a proline, and because cross peaks from T33 were not resolved in the ^1H COSY fingerprint region (Figure 3), M32 was not determined in the sequential $d_{\alpha N}$ walk. The M32 spin system was placed on the basis of a d_{NN} cross peak between M32 and L25 (Figure 6B), which arises because these two residues are located on adjacent strands of antiparallel β-sheet. F34 was assigned from a seven-residue sequential $d_{\alpha N}$ walk, F34–D40 (Figures 6A and 3S).

Long-range $d_{\alpha N(i,j+1)}$ or $d_{\alpha N(j,i+1)}$ NOE's, characteristic of amide protons on opposite strands of antiparallel β-sheet, were observed between the following residue pairs (as indicated by arrows in Figure 6B pointing to the peak positions of the corresponding residues): E10–V74, A12–I72, E73–Y93,

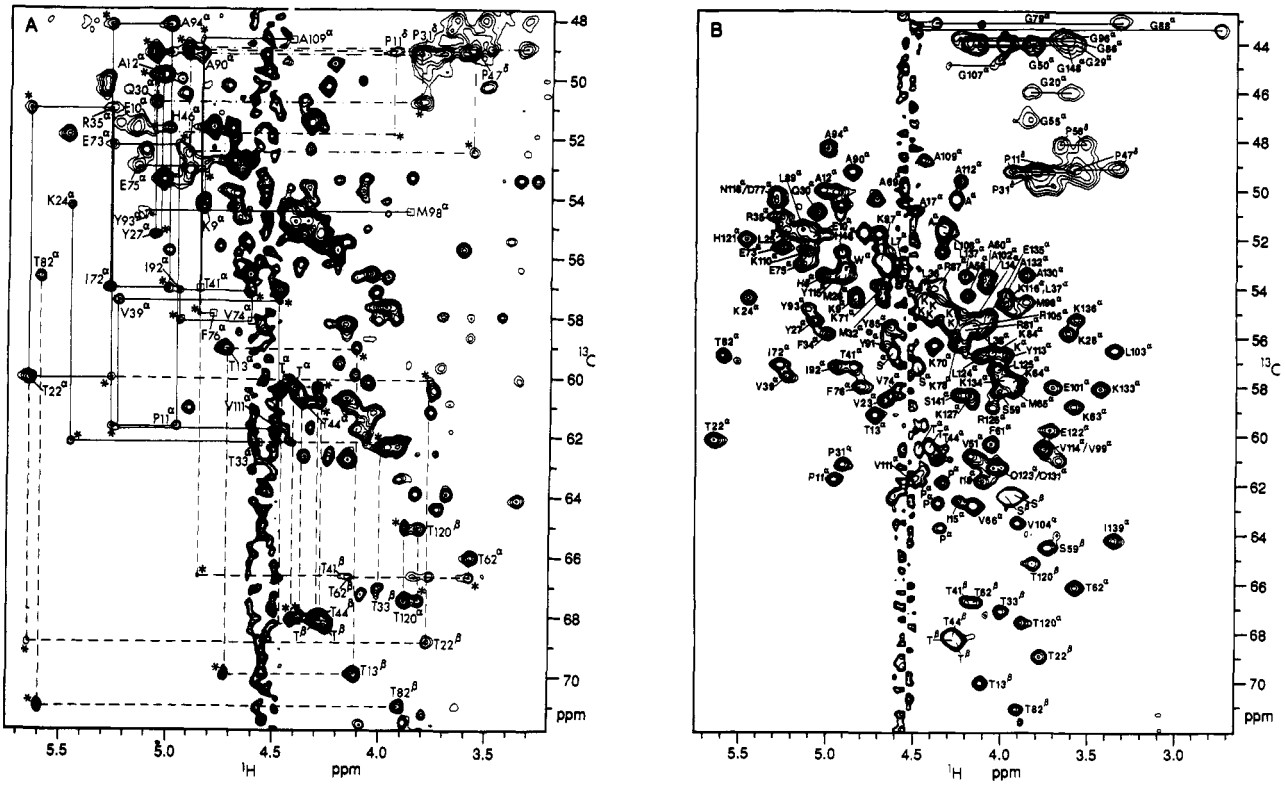

FIGURE 7: Assignment of ^{13}C signals in the $^1H\{^{13}C\}$SBC and $^1H\{^{13}C\}$SBC-NOE spectra of [26% UL ^{13}C]H124L in ^2H_2O solution. The ^{13}C carrier frequency was set at the center of aliphatic region. For each value of t_1, 4096 data points were collected in t_2. Prior to Fourier transformation, zero-filling in the t_1 dimension was applied to extend it to 2048 points. A Gaussian window function was used in t_2, and a shifted sine bell was applied in t_1. (A) Part of the aliphatic region of the 600-MHz $^1H\{^{13}C\}$SBC-NOE spectrum. A total of 426 increments were collected with 184 scans for each t_1 value. The NOE mixing time was 250 ms. All NOE relay cross peaks are denoted by asterisks. The positions of weak direct cross peaks are indicated by boxes. Long-range NOE connectivities between opposite strands are indicated by solid lines. Dashed lines represent Thr intraresidue NOE connectivities, and dotted-dashed lines indicate interresidue NOE's between the $^1H^\delta$ of proline and the $^1H^\alpha$ of the preceding residue. (B) Part of the aliphatic region of the 500-MHz $^1H\{^{13}C\}$SBC spectrum. A total of 400 increments were collected with 132 scans accumulated for each t_1. Assigned ^1H–^{13}C direct cross peaks are indicated by residue number and atom types.

E75–Y91, A94–K97, T13–M26, I15–K24, V23–F34, L25–M32, Y27–Q30, and D40–K110.

(2) Sequence-Specific Assignment of Backbone ^{15}N Signals. The assigned ^1H–^{15}N direct cross peaks of the residues within these three antiparallel β-sheets are indicated in Figure 4. These assignments were deduced from the ^1H NOESY (^1H_2O) spectrum of H124L and from the $^1H\{^{15}N\}$SBC-NOE spectrum of [95% UL ^{15}N}H124L. The ^1H–^{15}N connectivity region of the $^1H\{^{15}N\}$SBC-NOE spectrum contained short sequential d_{NN} connectivity patterns expected for reverse turns and a number of single-step ^{15}N-assisted d_{NN} connectivities between pairs of residues on opposite strands of β-sheet (Figure 4S, Supplementary Material). The $^1H^N$–$^1H^N$ connectivities from these spectra are in complete agreement with the sequential assignment pathways identified in the ^1H NOESY (^1H_2O) spectrum (Figure 6A,B). The 2D assigned ^1H–^1H and ^1H–^{15}N connectivities match those identified from slices of the 3D ^1H–^{15}N NOESY-HMQC spectrum (Wang et al., 1992).

(3) Sequence-Specific Assignment of ^{13}C Signals. A strong interstrand $d_{\alpha\alpha}(i,j)$ NOE connectivity is characteristic of an antiparallel β-sheet (Wüthrich et al., 1984; Wagner et al., 1986; Englander et al., 1987). Such NOE connectivities are readily observed in $^1H\{^{13}C\}$SBC-NOE spectra of a protein uniformly labeled with ^{13}C (Wang et al., 1990b). Figure 7A shows the region of the $^1H\{^{13}C\}$SBC-NOE spectrum recorded with [26% UL ^{13}C]H124L that should contain $^1H^\alpha$-$^{13}C^\alpha$ direct cross peaks, $^1H^\beta$–$^{13}C^\beta$ direct cross peaks (from threonines and serines), and $^1H^\alpha_i$–$^{13}C^\alpha_j$ and $^1H^\alpha_j$–$^{13}C^\alpha_i$ NOE-relay cross peaks.

As described by Wang et al. (1990b,c), several spin system types can be identified by analysis of $^1H\{^{13}C\}$SBC and $^1H\{^{13}C\}$SBC-NOE data. The $^1H^\alpha$–$^{13}C^\alpha$ and $^1H^\beta$–$^{13}C^\beta$ direct cross peaks from threonines are shown by dashed lines in Figure 7A. The alanine spin systems were identified by 2D ^1H homonuclear HOHAHA and $^1H\{^{13}C\}$MBC experiments (not shown). Nuclease H124L samples labeled selectively with individual [26% UL ^{13}C]-amino acids (Lys, Pro, Leu, Phe, or His) were investigated by 2D $^1H\{^{13}C\}$SBC NMR. The results of these experiments (spectra not shown) led to identification of the $^1H^\alpha$–$^{13}C^\alpha$ direct cross peaks of all these residues. Other $^1H^\alpha$–$^{13}C^\alpha$ direct cross peaks were identified from $d_{\alpha\alpha}(i,j)$ NOE information, spin system analyses, or $^1H^\alpha$ peak assignments. All the assigned ^1H–^{13}C cross peaks are indicated in Figure 7B.

Several pairs of $d_{\alpha\alpha}(i,j)$ NOE connectivities were observed (Figure 7A). These include interstrand NOE connectivities between the $^1H^\alpha$'s of I72 and A94, P11 and E73, A12 and Y27, K9 and E75, and T22 and R35. The $^1H^\alpha$–$^{13}C^\alpha$ direct cross peaks of M98, F76, and T41 are weak, and the direct cross peaks of A109, V74, and V111 are obscured by the residual water signal; their locations (Figure 7A) are indicated by boxes. In addition, $d_{\alpha\alpha}(i,j)$ NOE connectivities, which allowed us to confirm and extend the $^{13}C^\alpha$ assignments, were detected between the $^1H^\alpha$'s of several residue pairs: V74 and I92, Y93 and M98, F76 and A90, T41 and A109, and V39 and V111. The direct cross peak from T33 is missing in Figure 7. However, the $^1H^\alpha_i$–$^{13}C^\alpha_j$ NOE relay cross peak at (5.45, 62.2) ppm between K24 and T33 assigns the T33 $^{13}C^\alpha$ peak. NOE connectivities, detected between one $^1H^\delta$ of each of three proline residues and the $^1H^\alpha$ of the preceding residue (Figure 7A, dotted-dashed lines), show that the E10–P11, Q30–P31,

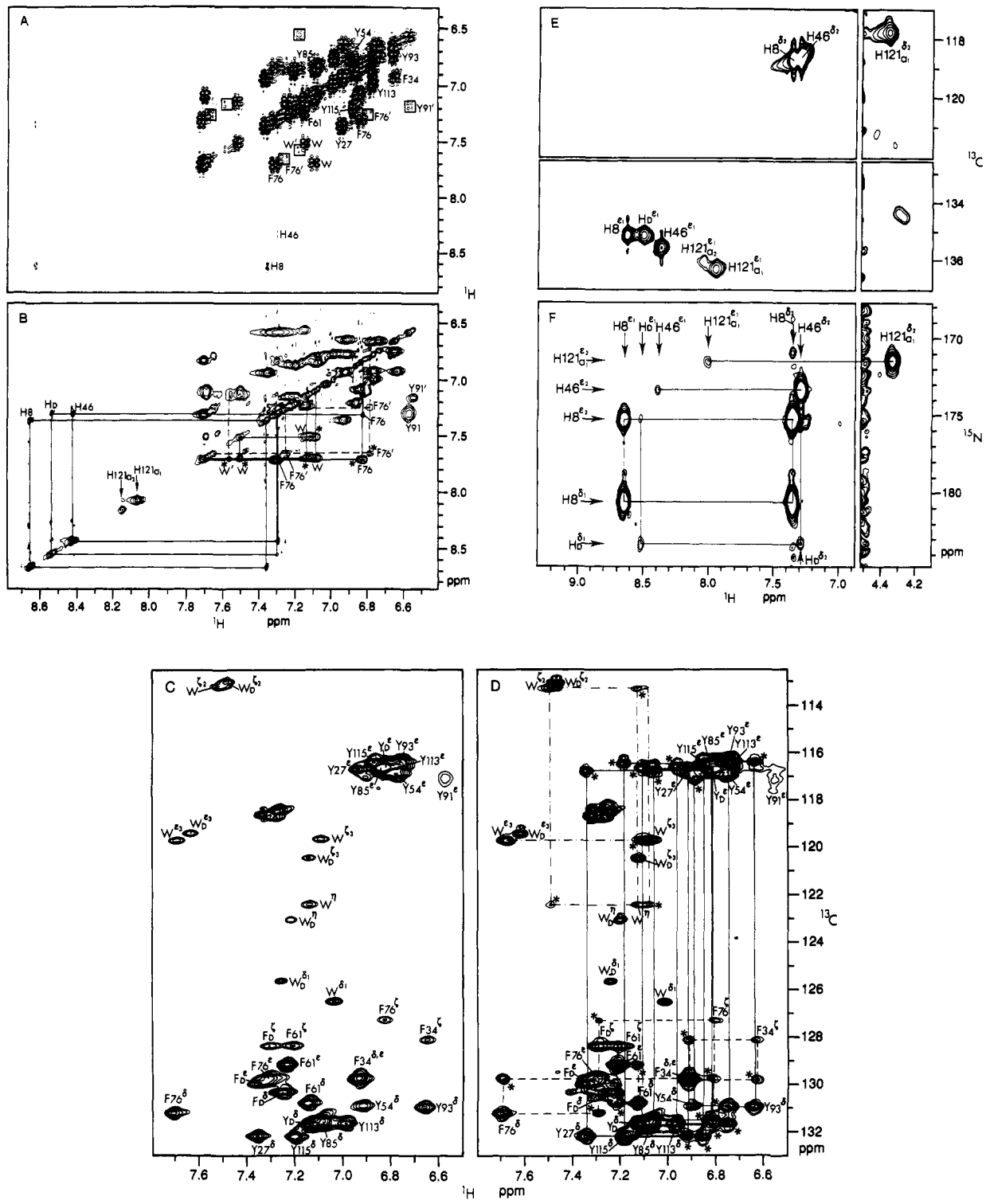

FIGURE 8: Assignments of the aromatic ring protons, protonated carbons, and nitrogens. (A) Aromatic region of the 500-MHz phase-sensitive ^{1}H{^{1}H} DQF-COSY spectrum of [na]H124L in ^2H_2O solution. (B) Aromatic region of the 500-MHz ^{1}H{^{1}H} HOHAHA spectrum of [na]H124L in ^2H_2O solution. The spectrum was recorded with 512 value in t_1 and 192 scans for each t_1 value. The spin-lock mixing time was 55 ms. Other acquisition parameters were identical with those given for DQF-COSY experiment. Shifted sine bell window functions were applied in both dimensions. Hartmann–Hahn relay cross peaks are denoted by asterisks. Cross peaks assigned to the a1 subconformation (Wang et al., 1990c) are boxed and labeled with primed numbers. (C) Part of the 600-MHz ^{1}H{^{13}C}SBC spectrum of [26% UL ^{13}C]H124L in ^2H_2O solution recorded with 288 blocks and 184 scans per t_1 value. The ^{13}C carrier frequency was set at the center of the aromatic region. (D) Part of the 500-MHz ^{1}H{^{13}C}SBC-NOE spectrum of [26% UL ^{13}C]H124L in ^2H_2O solution recorded with carrier frequency at the center of the aromatic region. A total of 268 blocks with 256 scans per t_1 were collected. The NOE mixing time was 200 ms. NOE relay cross peaks are indicated by asterisks. The spectral regions shown in panels C and D were selected to show cross peaks from tyrosine and phenylalanine residues. (E) 500-MHz ^{1}H{^{13}C}SBC spectrum of [26% UL ^{13}C]His-H124L in ^2H_2O solution recorded with the carrier frequency centered in the histidine region. A total of 166 blocks were collected with 256 scans per t_1 value. (F) Part of the 500-MHz ^{1}H{^{15}N}MBC spectrum of [95% UL ^{15}N]His-H124L in ^2H_2O solution. Data were recorded selectively for the histidine region in the ^{15}N dimension. A total of 188 blocks were collected with 256 scans for each t_1 value. The delay time for suppressing single-bond correlations was 5.56 ms. Assigned cross peaks in all above spectra are labeled with one-letter amino acid code, residue number, and atom type, except for W140 whose peaks are labeled with the letter alone. The subscript D denotes signals from a small amount of unfolded or degraded protein of unknown origin.

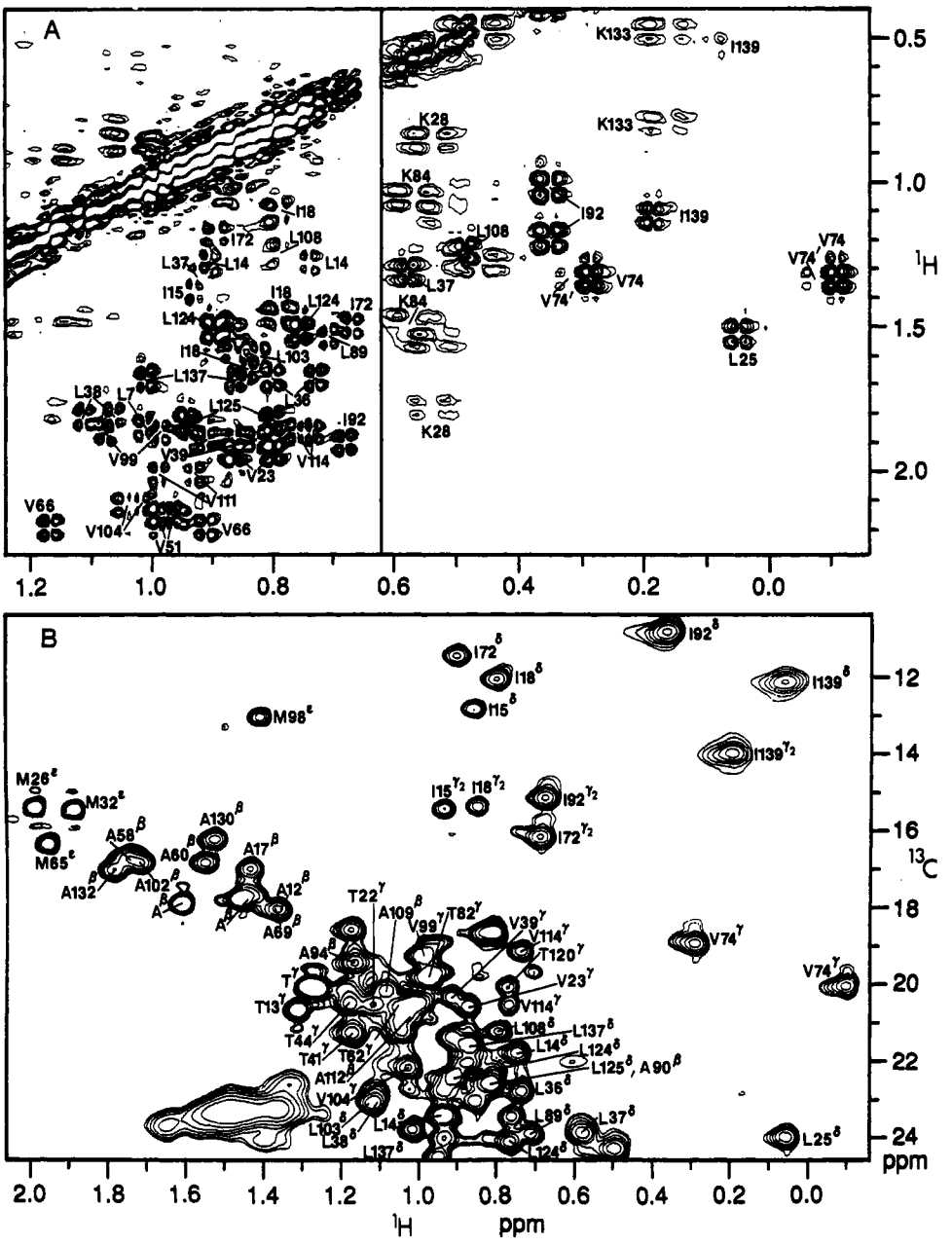

FIGURE 9: Part of the 500-MHz ^{1}H{^{13}C}MBC spectrum of [26% UL ^{13}C]H124L recorded for the aromatic region. A total of 366 t_1 increments were collected with 200 scans for each. The delay time for suppressing one-bond correlations was 2.78 ms, and the delay time for optimizing two- and three-bond correlations was 70 ms. The spectrum is presented in the mixed mode, and the final data size was identical to other ^{1}H–^{13}C heteronuclear experiments. Three-bond correlation cross peaks of tyrosine and phenylalanine residues are denoted by asterisks; those from W140 are labeled by "W".

and H46–P47 peptide bonds are trans. [Signals from the b2 minor conformational form of nuclease H124L, which is thought to have a cis H46–P47 peptide bond (Wang et al., 1990c), were not observed in the 2D spectra.]

Two Loops (Asp^{77} to Ala^{90} and Tyr^{113} to His^{121}) and a Bend (Lys^{70} to Lys^{71}): Sequence-Specific Assignment of Backbone ^{1}H–^{15}N Signals

The amino acid residues located in segments D77–A90 and Y113–H121 constitute two loops. The sequential $d_{\alpha N}$ walks through the loop segments and the single-step NOE between K70 and K71 are indicated by solid lines in Figure 6A. ^{1}H NOESY (Figure 6B) and ^{1}H{^{15}N}SBC-NOE (Figure 4S) data provided sequential d_{NN} connectivities for residues K70–K71, K78–G79, R81–T82, Y85–G86–R87, Y113–V114, and N119–T120. The base of the D77–A90 loop is defined by nonsequential NOE connectivities between T82 ^{1}H$^\alpha$ and L89 ^{1}H^N and between D83 ^{1}H^N and R87 ^{1}H^N (Figure 6A,B). The presence of a loop from A112 to H121 is indicated by nonsequential $d_{\alpha N}$ connectivities from K116 ^{1}H$^\alpha$ to N118 ^{1}H^N and N119 ^{1}H^N (Figure 6A). Assigned ^{1}H^N–^{15}N direct connectivity peaks from these loops are indicated in Figure 4.

^{1}H, ^{15}N, and ^{13}C Signals from Aromatic Rings

(1) ^{1}H Resonances. The aliphatic proton resonances of the 14 aromatic residues were assigned mainly from 2D ^{1}H NOESY (H_2O), 2D COSY (H_2O), and 3D ^{1}H–^{15}N NOESY-HMQC data. The ^{1}H$^\alpha$ resonances of Y85 and Y91 and the ^{1}H$^\beta$ resonances of Y54 were assigned by analysis ^{1}H NOESY (^2H_2O) data. The ^{1}H$^\alpha$–^{1}H$^\beta$ cross peaks of all the aromatic amino acid residues, except for that of Y54 which was not visible, are indicated in Figure 2. As described in the

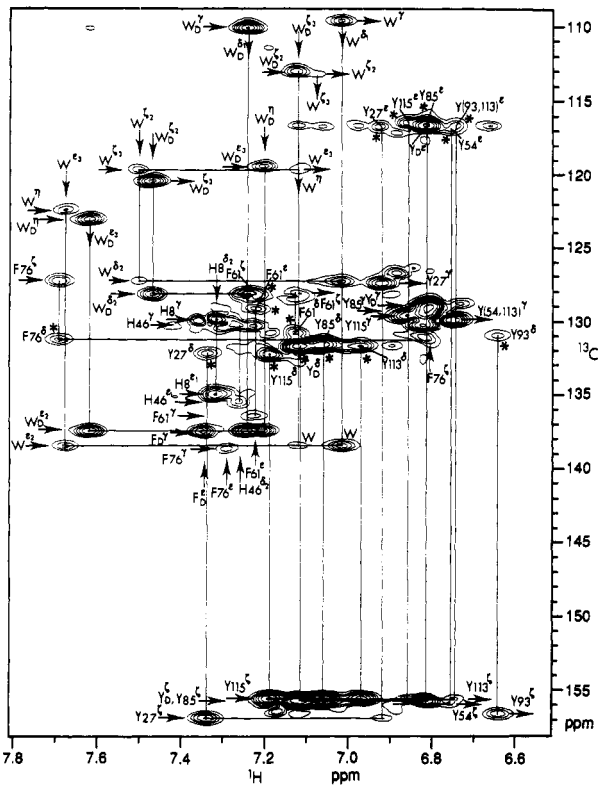

FIGURE 10: Assignments in the methyl region. (A) Methyl region of the 500-MHz $^{1}H\{^{1}H\}$DQF-COSY spectrum of [na]H124L in $^{2}H_2O$ solution. Labels indicate the positions of Val, Leu, and Ile cross peaks. (The two parts of the spectrum are presented at different contour levels.) (B) Methyl region of the 500-MHz $^{1}H\{^{13}C\}$SBC spectrum of [26% UL ^{13}C]H124L in $^{2}H_2O$. Labels indicate the positions of methionine, alanine, and threonine direct cross peaks and selected isoleucine, leucine, and valine peaks.

study of the nuclease H124L ternary complex (Wang et al., 1990c), NOE connectivities that link δ-proton resonances of the aromatic rings to their aliphatic β- or α-proton resonances can be found in $^{1}H\{^{13}C\}$SBC-NOE and ^{1}H NOESY ($^{2}H_2O$) spectra. Analysis of these regions of the spectra of uncomplexed nuclease H124L revealed $^{1}H^{\beta}$–$^{1}H^{\delta}$ and $^{1}H^{\alpha}$–$^{1}H^{\delta}$ NOE connectivities for the single tryptophan, all three phenylalanines, all seven tyrosines, and two of the three histidine residues (H8 and H46). Assignments of the aromatic protons of tryptophan, tyrosine, and phenylalanine are indicated in Figure 8A. Assignments to F76, Y91, and W140 in the a2 (minor) conformational form (indicated by primed residue numbers in the figures) are confirmed by cross peaks present in the ^{1}H HOHAHA ($^{2}H_2O$) spectrum (Figure 8B).

(2) ^{15}N and Protonated ^{13}C Resonances. Comparison of the aromatic ^{1}H assignments discussed above (Figure 8A) with 2D ^{1}H–^{13}C spectra led to ^{13}C assignments for the aromatic amino acid side chains. Figure 8 panels C and D show $^{1}H\{^{13}C\}$SBC and $^{1}H\{^{13}C\}$SBC-NOE spectra of [26% UL ^{13}C]-H124L in $^{2}H_2O$ solution (recorded selectively for the aromatic region). The $^{1}H^{\delta}$–$^{1}H^{\epsilon}$ NOE connectivities of the tyrosine ring, the $^{1}H^{\zeta}$–$^{1}H^{\epsilon}$ and $^{1}H^{\epsilon}$–$^{1}H^{\delta}$ NOE connectivities of phenylalanine ring and the ring proton NOE's of tryptophan are indicated by solid, dashed, and dotted-dashed lines, respectively. This analysis yielded unambiguous assignments of the Tyr $^{13}C^{\delta}$ and $^{13}C^{\epsilon}$ and Phe $^{13}C^{\delta}$, $^{13}C^{\epsilon}$, and $^{13}C^{\zeta}$ resonances.

The imidazole spin systems of the histidine residues (Wang et al., 1990c) were identified from $^{1}H\{^{1}H\}$DQF-COSY and HOHAHA (Figure 8A,B), $^{1}H\{^{13}C\}$SBC (Figure 8E), $^{1}H\{^{13}C\}$MBC (not shown), and $^{1}H\{^{15}N\}$MBC (Figure 8F) data. The assignments of the imidazole spin systems of H8 and H46

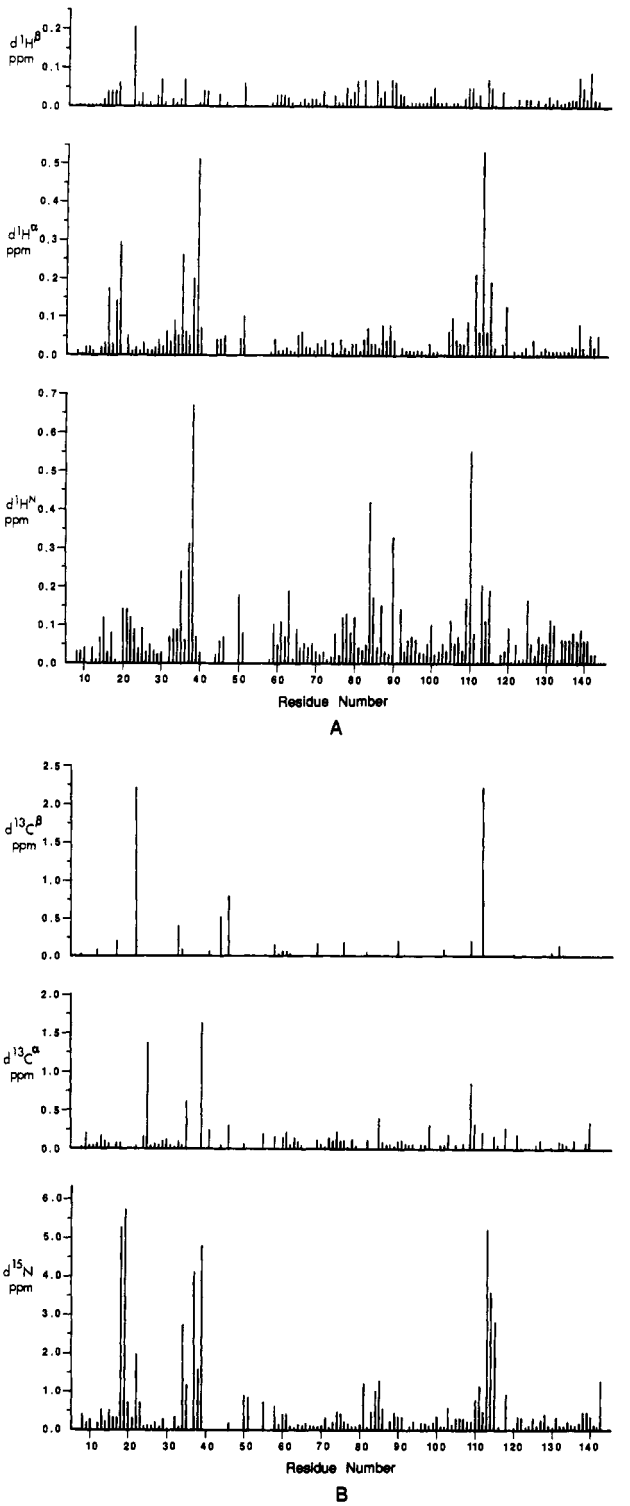

FIGURE 11: Diagrammatic representation of the chemical shift changes that accompany ternary complex formation. The absolute value (in ppm) of the assigned chemical shift in nuclease H124L minus that in (nuclease H124L)·pdTp·Ca^{2+} is plotted (vertical axis) versus the residue number (horizontal axis). (A) Chemical shift changes of $^{1}H^{N}$, $^{1}H^{\alpha}$, and $^{1}H^{\beta}$ versus the residue number. (B) Chemical shift changes of ^{15}N, $^{13}C^{\alpha}$, and $^{13}C^{\beta}$ versus the residue number.

are indicated in the $^{1}H\{^{1}H\}$ HOHAHA spectrum (Figure 8B). The ^{1}H–^{13}C direct cross peaks of the H8 and H46 rings (Figure 8E) were assigned by extending the $^{1}H^{\epsilon 1}$ and $^{1}H^{\delta 2}$ assignments. The $^{1}H^{\delta 2}$–$^{13}C^{\delta 2}$ direct cross peak of H121 is shifted into the aliphatic region by the ring current of Y91 (Wang et al., 1990c; Hinck et al., 1990). Figure 8F shows histidine $^{1}H^{\delta 2}$–$^{15}N^{\delta 1,\epsilon 2}$ and $^{1}H^{\epsilon 1}$–$^{15}N^{\delta 1,\epsilon 2}$ multiple-bond NOE

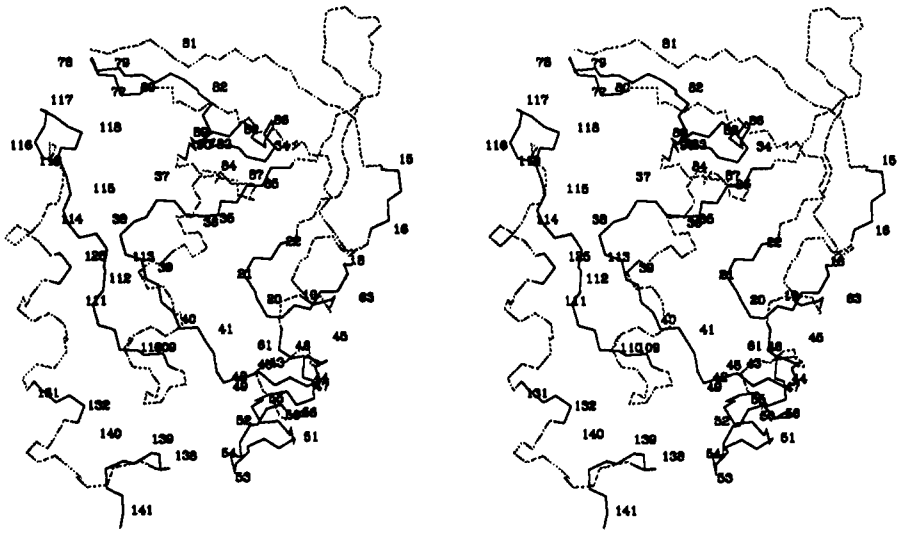

FIGURE 12: Stereoscopic representation of the backbone heavy atoms of the staphylococcal nuclease·pdTp·Ca^{2+} ternary complex, from the refined X-ray structure (Loll & Lattman, 1989); those residues that show the largest chemical shift changes on complex formation are highlighted.

connectivities in the $^1H\{^{15}N\}$MBC NMR spectrum which provide assignments of the $^{15}N^{\delta 1}$ peak of H8 and the $^{15}N^{\epsilon 2}$ peaks of H8, H46, and H121 in the a1 subconformation. (The $^1H^{\epsilon 1}$–$^{15}N^{\delta 1}$ and $^1H^{\delta 2}$–$^{15}N^{\delta 1}$ NOE connectivities of H46 and H121 were not observed.)

(*3*) *Nonprotonated Carbons.* Figure 9 shows the $^1H\{^{13}C\}$-MBC data (recorded selectively for aromatic resonances) of [26% UL ^{13}C]H124L. Tyrosine $^{13}C^{\zeta}$ resonances are centered around 156 ppm. The three-bond $^1H^{\delta}$–$^{13}C^{\zeta}$ and two-bond $^1H^{\epsilon}$–$^{13}C^{\zeta}$ correlations of five of the seven tyrosines were readily identified from their $^1H^{\delta}$ and $^1H^{\epsilon}$ assignments (Figure 9). Tyrosine $^{13}C^{\gamma}$ resonances are also located in a relatively well-resolved region, and the three-bond $^1H^{\epsilon}$–$^{13}C^{\gamma}$ correlations of five of the seven tyrosines provided $^{13}C^{\gamma}$ assignments.

Although the His $^{13}C^{\gamma}$ resonances are located in a relatively crowded region, the two-bond $^1H^{\delta 2}$–$^{13}C^{\gamma}$ correlations from H8 and H46 were detected (Figure 9). Only F76 showed a three-bond $^1H^{\epsilon}$–$^{13}C^{\gamma}$ correlation cross peak, but not F34 and F61. The tryptophan $^{13}C^{\gamma}$, $^{13}C^{\delta 2}$, and $^{13}C^{\epsilon 2}$ assignments were provided by $^1H^{\delta 1}$–$^{13}C^{\gamma}$, $^1H^{\delta 1,\beta 2}$–$^{13}C^{\delta 2}$, and $^1H^{\delta 1,\epsilon 3,\eta}$–$^{13}C^{\epsilon 2}$ correlations (Figure 9).

Methyl Group ^1H and ^{13}C Signals

The methyl proton resonances of valine, leucine, and isoleucine usually appear upfield of 1.0 ppm; those of alanine and threonine normally lie between 1.2 and 1.4 ppm; and those of methionine appear around 2.1 ppm (Wüthrich, 1986). Thus, the 2D ^1H–^1H region bounded by (−0.16–1.24, 0.4–2.3) ppm (Figure 10A) should contain valine $^1H^{\beta}$–$^1H^{\gamma 1,\gamma 2}$, leucine $^1H^{\gamma}$–$^1H^{\delta 1,\delta 2}$, and isoleucine $^1H^{\delta}$–$^1H^{\gamma 1}$ and $^1H^{\beta}$–$^1H^{\gamma 2}$ cross peaks. The ^1H HOHAHA spectrum (^2H_2O) of nuclease H124L (not shown) revealed the spin systems of all nine valines and three of the five isoleucines. Spin systems of the two remaining isoleucines were determined from $^1H\{^{13}C\}$SBC-NOE data (not shown). The methyl protons of 12 leucines were identified from 2D ^1H HOHAHA (^2H_2O), DQF-COSY (^2H_2O), and 3D ^1H–^{15}N NOESY-HMQC data (Wang et al., 1992). Assignments to the minor (a2) conformational state are indicated by primed symbols. The $^1H^{\gamma}$–$^1H^{\delta}$ and $^1H^{\gamma}$–$^1H^{\beta}$ cross peaks of K133, K28, and K84 show up in the methyl proton region (Figure 10A) as the result of ring current effects from W140, Y27, and Y85. The cross peaks of K133 were identified from the 2D ^1H HOHAHA (^2H_2O) and 3D ^1H–^{15}N NOESY-HMQC data; those of K28 and K84 were identified from 3D ^1H–^{15}N NOESY-HMQC data.

The ^1H–^{13}C direct cross peaks in the methyl regions of isoleucine, valine, leucine, alanine, threonine, and methionine should appear in the $^1H\{^{13}C\}$SBC spectral region bounded by (−0.16–2.06, 10.3–24.6) ppm (Figure 10B). The spin system assignments in the $^1H\{^{13}C\}$SBC-NOE spectrum determine the direct cross peaks for methyl group of 5 isoleucine, 7 threonine, and 14 alanine residues as indicated in Figure 10B. Several $^1H^{\delta}$–$^{13}C^{\delta}$ cross peaks of leucine were determined by the $^1H\{^{13}C\}$SBC-NOE experiment performed with uncomplexed [26% UL ^{13}C]Leu-H124L. Because the valine and leucine cross peaks are located in very crowded region, the remaining leucine cross peaks and most of the valine cross peaks were not distinguished in Figure 10B. The $^1H^{\epsilon}$–$^{13}C^{\epsilon}$ cross peaks of the four methionine residues (Figure 10B) are nearly in the same positions as the corresponding peaks in the $^1H\{^{13}C\}$SBC spectrum of [26% UL ^{13}C]Met-H124L in the ternary complex (Wang et al., 1990b), and they were assigned on the basis of this comparison.

Discussion

The chemical shift assignments for nuclease H124L are summarized in Table I (^1H resonances) and Table II (^{13}C and ^{15}N resonances). The present data on nuclease H124L can be compared closely with the previous results with the (nuclease H124L)·pdTp·Ca^{2+} ternary complex (Wang et al., 1990a–c), because the 2D data were collected under very similar experimental conditions and processed in the same way. Changes in the ^1H, ^{15}N, and ^{13}C chemical shifts of the backbone atoms upon complex formation are represented in Figure 12, which plots the absolute value of the chemical shift differences (in ppm) versus the residue number. The results show that backbone ^{15}N, $^1H^N$, $^1H^{\alpha}$, and $^{13}C^{\alpha}$ resonances in certain sections of the amino acid sequence show large shifts upon binding pdTp and Ca^{2+}. In particular those centered around G20, L37, G50, Y85, and Y113 are very sensitive to ternary complex formation. The chemical shift changes observed to accompany ternary complex formation are summarized in Table 1S.

We have compared the X-ray structure of unligated nuclease (Fox et al., 1991) with that of the ternary complex (Loll & Lattman, 1989). Upon superimposing the backbone atoms (N–C^{α}–C′) from L7 to S141, the backbone structures appear very similar with the exception of three segments: A17–T22, V39–P56, and A112–P117. The RMS deviation of these three

Table I: ^1H Resonance Assignments for Uncomplexed Staphylococcal Nuclease H124L at pH 5 and 45 °C[a]

residue	$^1H^N$	$^1H^\alpha$	$^1H^\beta$	$^1H^\gamma$	$^1H^\delta$	$^1H^\epsilon$	$^1H^\zeta$	$^1H^\eta$
A1								
T2								
S3								
T4								
K5								
K6								
L7		4.56	1.78	1.84	0.93, 1.01			
H8	8.86	5.03	3.26, 3.34		δ_2 7.34	ϵ_1 8.65		
K9	8.48	4.82	1.53					
E10	9.33	5.08	2.16					
P11		4.96*	2.44*, 2.54					
A12	8.13	5.02	1.34					
T13	8.08	4.73	4.12	1.30				
L14	9.15	4.15	1.95	1.25	0.73, 0.89			
I15	8.43	4.25	1.37	γ_1 1.36*; γ_2 0.92	0.83			
K16	8.08	4.42	1.76, 1.88	1.30*	1.68*			
A17	9.45	4.49	1.41					
I18	7.94	4.11	1.64	γ_1 1.08, 1.45 γ_2 0.84		0.78		
D19	8.51	4.26	2.08					
G20	8.63	3.60, 3.82						
D21	7.83	4.96						
T22	7.58	5.65	3.77	1.10				
V23	9.06	4.67	1.92	0.79, 0.85				
K24	9.48	5.45	1.99	1.40*	1.69*			
L25	9.42	5.24	1.78	1.52	0.03, 0.77*			
M26	9.54	4.89	1.76, 2.27			1.97		
Y27	9.08	5.07	3.01, 3.18		7.35	6.93		
K28	9.28	3.62	1.41, 1.78*	0.53*	0.84*			
G29	8.39	3.58, 4.14						
Q30	7.85	5.06	2.08, 2.19	2.40*				
P31		4.90*	1.94, 2.05*					
M32	9.57	4.68	2.01, 2.12			1.89		
T33	8.95*	4.58	3.99	1.03				
F34	9.60	4.99	2.87		6.92	6.92	6.64	
R35	9.60	5.25	1.85					
L36	8.26*	4.41*		1.65	0.72, 0.79			
L37	7.76*	3.97*		1.29	0.57, 0.92			
L38	8.65*	4.10*		1.80	1.06, 1.11			
V39	7.01	5.23	1.88	0.82, 0.90				
D40	8.85	5.15	2.35, 2.52					
T41		4.84	4.19	1.15				
P42								
E43								
T44	8.37	4.42	4.30	1.16				
K45	8.19*	4.28*						
H46	8.41	4.94	3.11, 3.18		δ_2 7.28	ϵ_1 8.33		
P47								
K48								
K49								
G50	8.41*	3.81, 4.14						
V51	7.94*	4.20*	2.14*	0.96, 0.98				
E52								
K53								
Y54	8.10*	4.42*			6.89	6.76		
G55	8.65	3.87, 3.97*						
P56								
E57								
A58	8.83	4.18	1.73					
S59	8.21	4.02*	3.71*					
A60	8.18	4.08	1.54					
F61	8.26	4.06	3.17, 3.34		7.14	7.23	7.23	
T62	8.65	3.58	4.14	1.03				
K63	7.86	3.58	1.78					
K64	7.96	3.94	1.74					
M65	7.74	3.93	1.79			1.95		
V66	8.18	4.16	2.17	0.90, 1.16				
E67	8.73	3.97	2.07					
N68	7.36	4.71	2.76, 2.81					
A69	6.73	4.53*	1.34					
K70	10.14	4.38	2.04					
K71	8.87	4.68	1.70, 1.84					
I72	8.89	5.27	1.89	γ_1 1.17; γ_2 0.67	0.89			
E73	8.81	5.26	1.74					
V74	9.56	4.59	1.32	−0.13, 0.27				
E75	8.90	5.15	2.90					
F76	8.77	4.81	2.93		7.70	7.30	6.82	

Table I (Continued)

residue	$^1H^N$	$^1H^\alpha$	$^1H^\beta$	$^1H^\gamma$	$^1H^\delta$	$^1H^\epsilon$	$^1H^\zeta$	$^1H^\eta$
D77	9.38	5.29	3.78					
K78	10.44	4.25	1.93					
G79	8.56	3.31, 4.38						
Q80	8.56	4.17	2.07*					
R81	8.59	4.17						
T82	7.36	5.60	3.91	0.96				
D83	8.70	4.72	2.65*					
K84	8.20*	4.05*	1.64	0.56	1.04			
Y85	7.98	4.62	2.81		7.07	6.84		
G86	8.14	3.63, 4.23						
R87	8.52	4.47						
G88	8.83*	2.73, 4.48						
L89	8.34	5.13	1.77	1.51	0.70			
A90	7.65	4.85	0.81					
Y91	9.02	4.65	3.43		7.30	6.58		
I92	7.93	4.95	1.49	γ_1 0.97, 1.08; γ_2 0.66		0.34		
Y93	9.55	5.10	2.84		6.65	6.74		
A94	9.29	4.99	1.14					
D95	9.72	4.44	2.75					
G96	9.34	3.66, 4.23						
K97	7.89	4.67	1.86, 1.75					
M98	9.25	3.85	1.99			1.40		
V99	10.15	3.74	1.86	0.98, 1.07				
N100	9.68	4.06	2.74, 2.90					
E101	6.17	3.70	1.94, 2.26					
A102	7.87	4.08*	1.70					
L103	8.05	3.34	1.70	1.59	0.81, 1.12*			
V104	6.84	3.92	2.10	1.10, 1.04				
R105	9.14	4.13	2.01					
Q106	7.20	4.34	1.47, 2.00	2.38				
G107	8.10	4.01, 4.28						
L108	7.79	4.36	1.47	1.23	0.48, 0.78			
A109	7.09	4.44	1.08					
K110	8.14	5.11	1.88					
V111	9.05	4.50*	2.00	0.92, 0.98				
A112	7.92	4.23	1.01					
Y113	7.98	3.97	2.95*, 3.04		6.97	6.76		
V114	7.63	3.75	1.86	0.72, 0.75				
Y115	8.78	4.84	3.05		7.20	6.87		
K116	8.65	3.97	1.76					
P117								
N118	8.60	5.29	3.08					
N119	8.13	4.91						
T120	10.63	3.88	3.81	0.76				
H121	6.93	5.48	2.35, 3.26		δ_2 4.33	ϵ_1 7.91		
E122	7.58	3.71	1.98*, 2.21					
Q123	8.86	4.01	1.99, 2.14					
L124	7.78	4.10	1.80	1.50	0.75, 0.89			
L125	7.84	4.03	1.88	1.81	0.79, 0.93			
R126	8.95	4.04	1.98					
K127	8.17	4.16	2.04					
S128	7.82	4.32	4.10					
E129	8.52	3.93	2.21					
A130	7.99	3.86	1.51					
Q131	7.56	4.01	2.21					
A132	7.95	3.97	1.77					
K133	8.16	3.42	0.78, 1.26	0.14	0.46			
K134	7.83	3.98	1.96					
E135	7.65	4.07	2.05					
K136	7.86	3.57	2.08					
L137	7.68	4.21	1.54	1.67	0.85; 1.00			
N138	9.06	3.93	2.85					
I139	8.44*	3.35	1.10	γ_1 0.51; γ_2 0.17	0.05			
W140	7.83	4.91	2.85, 3.71		δ_1 7.01	ϵ_3 7.68	ζ_2 7.51; ζ_3 7.09	7.13
S141	8.05	4.24	4.15*					
E142	7.92	4.45*	1.97, 2.20*	2.38*				
D143	8.30	4.70	2.70, 2.78*					
N144								
A145								
D146								
S147								
G148								
Q149								

[a] Results from the 3D ^1H–^{15}N NOESY-HMQC experiment are indicated by asterisks (*); $^1H^N$ chemical shifts were obtained in H_2O at pH 5.1; all others were obtained in ^2H_2O at pH* 5.5.

Table II: ^{15}N and ^{13}C Resonance Assignments for Uncomplexed Staphylococcal Nuclease H124L at pH 5 and 45 °C[a]

residue	^{15}N	$^{13}C^{\alpha}$	$^{13}C^{\beta}$	$^{13}C^{\gamma}$	$^{13}C^{\delta}$	$^{13}C^{\epsilon}$	$^{13}C^{\zeta}$	$^{13}C^{\eta}$	$^{15}N^{\epsilon 2}$	$^{15}N^{\delta 1}$
A1										
T2										
S3										
T4										
K5										
K6										
L7		53.3								
H8	119.0	53.4	29.5	129.9	δ_2 118.7	ϵ_1 135.1			175.2	180.7
K9	124.8	54.3								
E10	123.8	51.9								
P11		61.7			49.2					
A12	120.9	50.0	18.0							
T13	110.3	59.1	70.0	20.7						
L14	126.3	55.2		25.4	21.8, 23.4					
I15	125.9	62.6		γ_2 15.3	12.8					
K16	115.2									
A17	130.3	50.8	17.0							
I18	119.6	61.8		γ_2 15.3	11.9					
D19	125.0									
G20	104.7	46.0								
D21	111.6									
T22	116.1	60.1	68.9	20.6						
V23	120.5	58.5		18.6, 20.6						
K24	128.1	54.3								
L25	128.0	51.5			24.0					
M26	123.0	53.4				15.3				
Y27	130.6	55.3		127.4	132.2	116.8	156.9			
K28	128.3	55.8								
G29	103.3	44.0								
Q30	120.2	50.8								
P31		61.1			49.3					
M32	126.7	54.3				15.4				
T33	124.6	62.2	67.1							
F34	124.0	55.8	40.9		129.7	129.7	128.1			
R35	126.7	51.1								
L36		53.8		26.6	22.8, 25.0					
L37	127.0	54.6		26.2	23.9, 25.3					
L38	114.1	55.7			23.2, 25.5					
V39	109.4	57.5		18.6, 20.3						
D40	123.1									
T41		57.1	66.7	21.3						
P42					49.1					
E43	122.7									
T44	114.6	60.9	68.1	20.6						
K45										
H46	120.0	52.5	28.2	130.2	δ_2 118.6	ϵ_1 135.6			173.3	
P47					49.1					
K48										
K49										
G50	111.3	44.1								
V51	119.4	60.8								
E52										
K53										
Y54				129.9	130.9	117.0	155.9			
G55	110.1	47.1								
P56					48.1					
E57										
A58	125.3	54.3	16.7							
S59	112.6	58.1	64.4							
A60	123.8	53.5	16.8							
F61	122.5	60.3	38.3	136.4	130.8	129.1	128.4			
T62	120.9	66.1	66.7	20.7						
K63	120.7	58.8								
K64	118.2	57.7								
M65	117.1	58.1				16.3				
V66	108.7	62.8								
E67	121.7									
N68	114.4									
A69	122.2	49.9	18.0							
K70	126.3	56.3								
K71	122.2	53.9								
I72	129.8	57.1		γ_2 16.1	11.3					
E73	124.1	52.3								
V74	118.6	58.2		18.9, 20.0						
E75	127.9	53.0								
F76	127.6	57.9	38.4	138.6	131.2	129.7	127.3			
D77	124.3	50.4								

Table II (Continued)

residue	^{15}N	$^{13}C^{\alpha}$	$^{13}C^{\beta}$	$^{13}C^{\gamma}$	$^{13}C^{\delta}$	$^{13}C^{\epsilon}$	$^{13}C^{\zeta}$	$^{13}C^{\eta}$	$^{15}N^{\epsilon 2}$	$^{15}N^{\delta 1}$
K78	119.9	56.3								
G79	111.7	43.1								
Q80	125.7									
R81	122.5	55.6								
T82	107.7	56.7	71.1	19.8						
D83	121.8									
K84	117.7	56.6								
Y85	119.7	55.5		129.4	131.6	116.7	155.7			
G86	109.2	43.9								
R87	122.2	53.7								
G88	109.3	43.4								
L89	126.5	51.6			23.9					
A90	121.3	49.2	22.6							
Y91	123.3	56.3				117.2				
I92	123.5	57.1		γ_2 15.1	10.7					
Y93	127.2	54.8			130.9	116.4	156.6			
A94	126.8	48.3	19.4							
D95	128.2									
G96	103.9	43.7								
K97	122.4	52.8								
M98	127.7	54.5			12.9					
V99	136.7	60.5		19.3						
N100	109.3									
E101	113.5	58.0								
A102	123.6	53.8	16.8							
L103	116.9	56.5			23.1					
V104	117.3	63.5		20.2						
R105	123.9	55.5								
Q106	113.1									
G107	107.8	44.9								
L108	116.1	51.9			21.3, 24.3					
A109	114.4	48.8	20.2							
K110	118.9	52.5								
V111	123.4	61.9								
A112	132.5	49.6	20.8							
Y113	116.5	56.8		129.9	131.7	116.6	155.5			
V114	123.8	60.5		19.1, 20.6						
Y115	128.3	53.5		129.6	132.2	116.5	155.6			
K116	126.2	54.6								
P117										
N118	128.5	50.1								
N119	118.6	50.6								
T120	124.6	67.5	65.1	20.1						
H121	112.9	51.9			δ_2 117.8	ϵ_1 136.3			171.5	
E122	121.2	59.7								
Q123	118.4									
L124	122.1	56.7		25.6	22.4, 24.1					
L125	119.9	57.2		27.7	22.6					
R126	119.8	58.8								
K127	123.2	58.3								
S128	118.8									
E129	125.7									
A130	120.6	53.4	16.2							
Q131	119.1									
A132	123.9	54.2	17.0							
K133	118.2	58.0								
K134	123.1	57.7								
E135	117.3	55.1								
K136	117.6	55.2								
L137	118.2	53.5		25.1	21.6, 23.8					
N138	120.0									
I139	125.0	64.2		γ_2 13.9	12.0					
W140	120.8	53.2	28.4	109.7	δ_2 127.2; δ_1 126.5	ϵ_3 119.7; ϵ_2 138.3	ζ_3 119.7; ζ_2 113.3	η 122.2		
S141	116.8	58.3								
E142	122.0									
D143	121.4									
N144										
A145										
D146										
S147										
G148										
Q149										

[a] All ^{13}C data were collected at pH* 5.5 in ^2H_2O solution; single-bond correlation ^{15}N data were collected at pH 5.1 in H_2O solution; multiple-bond correlation ^{15}N data were collected at pH* 5.5 in ^2H_2O solution.

segments is 1.18 Å as compared to 0.24 Å for the rest of the molecule. [The overall RMS deviation for the whole molecule (residues L7–S141) is 0.63 Å.] These segments are the ones that show the largest chemical shift changes (Table 1S; Figure 11). Thus the NMR and X-ray results on the location of backbone structural changes upon complex formation are in excellent agreement.

The ^1H and ^{13}C resonances of several side chains exhibit large chemical shift changes upon ternary complex formation (Table 1S; Figure 11). Those of Y113 and Y115 as well as V39 can be attributed to direct effects since these side chains are located at the pdTp-binding site. Those of I18 and T22, which are in the neighborhood of the Ca^{2+}-binding site, may also be direct effects.

The positions of residues that show large chemical shift changes on complex formation are highlighted in the X-ray structure of the ternary complex (Figure 12). The X-ray structure of the nuclease·pdTp·Ca^{2+} ternary complex shows distorted octahedral coordination of Ca^{2+} to the side-chain carboxyl oxygens of D21, D40, and E43 and to the backbone carbonyl oxygen of T41. In addition, one of the oxygens of the 3′-phosphate of pdTp receives a hydrogen bond from the phenolic hydroxyl of Y85. The oxygens of the 5′-phosphate of pdTp form two pairs of hydrogen bonds to two of the nitrogens of the guanidinium ions of R87 and R35 (Tucker et al., 1979a). The guanidinium groups of R87 and R35 form bridged hydrogen-bonding networks to the carboxyl oxygen of D83 and to the main-chain carbonyl oxygens of L36 and V39 (Tucker et al., 1979a). A number of main-chain to main-chain hydrogen bonds and main-chain to side-chain hydrogen bonds (Loll et al., 1989) also exist between residues in the segments that show large resonance shifts on inhibitor binding. These hydrogen-bonding networks appear to provide the mechanism for propagating changes at the binding site to other residues in the molecule.

The NMR results show that D19 and D21 are located in an α-helical turn of the second β-sheet. Residues R35, L36, and V39 link the C-terminus of one of the strands in the second β-sheet with the N-terminus of a strand in third β-sheet. The observed NOE's between L37, L38, and V39 reveal that the backbone of this segment is bent. V39 also participates in the strand of the third β-sheet that includes D40 and T41. D83, Y85, and R87 are located in the D77–A90 loop. E43 is located in the very flexible P42–E57 loop; we have made only a few assignments to residues in this loop (Figure 11). Many of the residues not in contact with pdTp or Ca^{2+} that show large chemical shift changes on ligation are located in loops whose backbones may be relatively more flexible than the backbone in other parts of the enzyme. Changes in hydrogen-bonding of residues involved in binding pdTp and Ca^{2+} may induce torsion angle changes in these backbone segments.

Conformational changes occur not only at the binding site but also in neighboring segments. A109, K110, and V111 show large chemical shift changes upon pdTp and Ca^{2+} binding. Together with A112 they form a strand that is antiparallel to the L38–V39–D40–T41 strand of the third β-sheet. The mechanism for producing these changes may be envisioned as follows. Ligand binding probably induces backbone torison angle changes in the L38–V39–D40–T41 segment. These are transmitted to the A109–A112 segment, which must adopt appropriate changes in order to maintain the antiparallel β-sheet structure. These structural accommodations lead to resonance shifts from residues in the A109–K110–V111 segment. Binding site residues Y113 and Y115 form part of the Y113–H121 loop. The crystallographic data (Loll et al., 1989) also suggest that main-chain to side-chain hydrogen bonds link the Y113–H121 and D77–A90 loops. These hydrogen bonds may provide a mechanism for transmitting changes in the backbone of the D77–A90 loop to the Y113–H121 loop.

Conclusion

Accurate chemical shift determinations from 3D and 4D NMR data will not be possible unless a practical means is found for increasing the digital resolution of such spectra. As shown here, one can use higher dimension spectra for connectivity determination (sequential or intraresidue) and then refine the chemical shift determinations by retracing the connectivities in appropriate 2D spectra.

In this report, we have compared chemical shifts obtained from uncomplexed nuclease H124L with those of the nuclease·pdTp·Ca^{2+} ternary complex. Large shifts are experienced not only by the residues involved in binding of pdTp and Ca^{2+} but also by residues of neighboring segments. Inhibitor binding appears to induce torsion angle changes in the backbone of four relatively flexible regions of nuclease H124L: the D77–A90 loop, the Y113–H121 loop, the P42–E57 loop, and the R35–V39 segment, which links strands from two different β-sheet structures: residues A12–R35 from the larger β-sheet and residues L38–T41 and A109–A112 from the smaller β-sheet. Tertiary structural changes in nuclease H124L that accompany inhibitor binding in solution will be investigated further through analysis of changes in NOE's and coupling constants of the assigned resonances.

Acknowledgments

We thank Dr. Robert O. Fox for supplying coordinates for the crystal structure of unligated staphylococcal nuclease (wild type) in advance of their publication.

Supplementary Material Available

Figure 1S showing $d_{\alpha N}$ NOE connectivities corresponding to the three α-helices observed in the ^1H NOESY(^1H_2O) spectrum; Figure 2S showing three long ^{15}N-assisted sequential d_{NN} walks in the ^1H–^{15}N connectivity region of the ^1H-{^{15}N}SBC-NOE spectrum; Figure 3S showing the $d_{\alpha N}$ sequential walks in the ^1H NOESY (^1H_2O) spectrum that correspond to the three antiparallel β-sheet structures; Figure 4S showing ^{15}N-assisted d_{NN} NOE connectivities in the ^1H-{^{15}N}SBC-NOE spectrum assigned to the three antiparallel β-structures and loops; and Table 1S listing the ^1H, ^{13}C, and ^{15}N chemical shift changes that accompany ternary complex formation (9 pages). Ordering information is given on any current masthead page.

Registry No. Ca^{2+}, 7440-70-2; pdTp, 2863-04-9; Staphylococcal nuclease, 9013-53-0.

References

Alexandrescu, A., Ulrich, E. L., & Markley, J. L. (1989) *Biochemistry 28*, 230–236.

Anil Kumar, Ernst, R. R., & Wüthrich, K. (1980) *Biochem. Biophys. Res. Commun.* 95, 1–6.

Bax, A., & Davis, D. R. (1985) *J. Magn. Reson. 65*, 355–360.

Bax, A., & Drobny, G. (1985) *J. Magn. Reson. 61*, 306–320.

Bax, A., & Summers, M. F. (1986) *J. Am. Chem. Soc. 108*, 2093–2094.

Bodenhausen, G., Kogler, H., & Ernst, R. R. (1984) *J. Magn. Reson. 58*, 370–388.

Cunningham, L., Catlin, B. W., & Privat de Garilhe, M. (1956) *J. Am. Chem. Soc. 78*, 4642-4645.
Englander, S. W., & Wand, A. J. (1987) *Biochemistry 26*, 5953-5958.
Hinck, A. P., Loh, S. N., Wang, J., & Markley, J. L. (1990) *J. Am. Chem. Soc. 112*, 9031-9034.
Hynes, T. R., & Fox, R. O. (1991) *Proteins: Struct., Funct., Genet. 10*, 92-105.
Loll, P. J., & Lattman, E. E. (1989) *Proteins: Struct., Funct., Genet. 5*, 183-201.
Markley, J. L., & Jardetzky, O. (1970) *J. Mol. Biol. 50*, 223-233.
Rance, M., Sørensen, W. W., Bodenhausen, G., Wagner, G., Ernst, R. R., & Wüthrich, K. (1983) *Biochem. Biophys. Res. Commun. 117*, 479-485.
Richardson, J. S. (1981) *Adv. Protein Chem. 34*, 167-339.
Shon, K., & Opella, S. J. (1989) *J. Magn. Reson. 82*, 193-197.
Sklenar, V., & Bax. (1987) *J. Magn. Reson. 71*, 379-383.
Torchia, D. A., Sparks, S. W., & Bax, A. (1989) *Biochemistry 28*, 5509-5524.
Tucker, P. W., Hazen, E. E., Jr., & Cotton, F. A. (1979a) *Mol. Cell. Biochem. 23*, 3-16.
Tucker, P. W., Hazen, E. E., Jr., & Cotton, F. A. (1979b) *Mol. Cell. Biochem. 23*, 67-86.
Ulrich, E. L., Markley, J. L., & Kyogoku, Y. (1989) *Protein Sequences Data Anal. 2*, 23-37.
Wagner, G. (1983) *J. Magn. Reson. 55*, 151-156.
Wagner, G., Neuhaus, D., Wörgötter, E., Vasak, M., Kagi, J. M. R., & Wüthrich, K. (1986) *J. Mol. Biol. 187*, 131-135.
Wang, J., LeMaster, D. M., & Markley, J. L. (1990a) *Biochemistry 29*, 88-101.
Wang, J., Hinck, A. P., Loh, S. N., & Markley, J. L. (1990b) *Biochemistry 29*, 102-113.
Wang, J., Hinck, A. P., Loh, S. N., & Markley, J. L. (1990c) *Biochemistry 29*, 4242-4253.
Wang, J., Mooberry, E. S., Walkenhorst, W. F., & Markley, J. L. (1992) *Biochemistry* (preceding paper in this issue).
Wüthrich, K. (1986) *NMR of Proteins and Nucleic Acids*, Wiley, New York.
Wüthrich, K., Billeter, M., & Braun, W. (1984) *J. Mol. Biol. 180*, 715-740.

Factors Affecting γ-Chain Multimer Formation in Cross-Linked Fibrin†

Kevin R. Siebenlist* and Michael W. Mosesson
University of Wisconsin Medical School, Milwaukee Clinical Campus, Sinai Samaritan Medical Center, Milwaukee, Wisconsin 53233

Received July 1, 1991; Revised Manuscript Received September 12, 1991

ABSTRACT: The major covalently linked multimolecular D fragments found in plasmic digests of factor XIIIa cross-linked fibrin formed under physiological pH and ionic strength conditions consist of D dimers, D trimers, and D tetramers. These fragments are linked by ε-amino-γ-glutamyllysine bonds in the carboxy-terminal regions of their γ chains, which had originated in the cross-linked fibrin as γ dimers, γ trimers, and γ tetramers, respectively. In this study, factors affecting the degree and rate of formation of these three classes of cross-linked γ chains were determined by analyzing the D-fragment content of plasmic digests of cross-linked fibrin that had been sampled after all γ-chain monomers had been consumed in the cross-linking process. D trimers and D tetramers, expressed as a proportion of the total D-fragment content, both increased at the expense of the D-dimer population as a function of increasing factor XIII concentration, the time of cross-linking, or the $CaCl_2$ concentration. Their levels decreased as the ionic strength was raised by NaCl addition. However, the ionic strength effect could be reversed by concomitantly raising the $CaCl_2$ concentration. Digests of clots prepared from recalcified fresh citrated plasma also contained each type of cross-linked D fragment, and the proportion of D trimers and D tetramers in the digest increased with increasing clot incubation time. These results indicate that γ-trimer and γ-tetramer formation is a dynamic physiological process. Such cross-linked trimeric and tetrameric γ-chain structures may function in vivo to stabilize the fibrin matrix at interfiber contacts and/or at branch points, thereby enhancing mechanical strength, elasticity, and/or clot resistance to fibrinolysis.

Following thrombin-catalyzed conversion of fibrinogen to fibrin, polymer assembly commences with formation of double-stranded fibrils in which fibrin molecules associate by noncovalent intermolecular interactions between the outer D domains and the central E domains (Blombäck et al., 1978; Laudano & Doolittle, 1978, 1980; Shainoff & Dardik, 1979, 1983; Olexa & Budzynski, 1980) forming a staggered overlapping fibrillar array (Ferry, 1952; Stryer et al., 1963; Krakow et al., 1972; Hantgan & Hermans, 1979; Fowler et al., 1981; Williams, 1981, 1983). The resulting two-stranded fibrils subsequently associate laterally, forming thick fibers that constitute the major structural elements of the branched three-dimensional fibrin matrix (Carr et al., 1977; Hantgan & Hermans, 1979; Hantgan et al., 1980, 1983; Hermans & McDonagh, 1982; Erickson & Fowler, 1983; Hewat et al., 1983). Multiple factors affect the ultimate structure of the fibrin matrix. Rapid assembly and thick fibrin fibers result when clotting occurs at or below physiological ionic strength (Ferry & Morrison, 1947; Hangtan et al., 1980, 1983; Müller et al., 1984; Carr et al., 1986) and when Ca^{2+} is included in the reaction medium (Boyer et al., 1972; Okada & Blombäck, 1983; Carr et al., 1986). Slowing the conversion of fibrinogen

† This investigation was supported by NHLBI Program Project Grant HL-28444.
* Address correspondence to this author at the Sinai Samaritan Medical Center, Winter Research Building, 836 North 12th St., Milwaukee, WI 53233.

0006-2960/92/0431-936$03.00/0